Growth of parametric fields in (2+1)-photon laser ionization of atomic oxygen

Merle E. Riley
Sandia National Laboratories, Albuquerque, New Mexico 87185
(Received 18 October 1989)

The multiphoton excitation of an atom by a strong pulsed laser field creates a transient inversion of the pumped, excited level with respect to a lower-lying intermediate level. This results in a coupled time-and-distance traveling-wave situation appropriate for the growth of auxiliary radiation fields that are coupled to the excited, intermediate, and ground levels. Under certain circumstances these fields can suppress the multiphoton excitation process. The two-photon pumping of a ground ^3P level of O to the first excited ^3P level and ionization to the continuum by the same field are analyzed for the growth of amplified spontaneous emission and parametric four-wave mixing. A threshold growth condition is used to interpret the numerical solutions of the appropriate Maxwell-Bloch equations. A novel transition from exponential to linear growth of the parametric waves is observed in the calculations.

I. INTRODUCTION

Laser fields with intensities on the order of GW/cm^2 are useful for ionizing atoms by means of multiphoton transitions. The natural selectivity of the excitation process, combined with detection of the ions, makes a useful atomic measurement technique. Atomic oxygen is the dominant species in the high atmosphere and is the specific concern of this work. One possible scheme for ionizing O is to apply a two-photon resonant field of 226 nm wavelength. The ground ^3P levels are pumped to the first excited ^3P levels and ionized to the continuum by the same photons. This is commonly referred to as a (2+1)-photon process as the first transition is two-photon, followed by a single-photon transition.

The recent work of Dixit, Levin, and McKoy[1] (DLM) presents quantum-defect calculations of the O atomic data and ionization dynamics of the (2+1)-photon process.

The topic of concern here is the growth of auxiliary radiation fields along a channel of ionization created by the 2+1 pumping. This is a combined time-and-distance evolution problem which is effectively one dimensional due to the pulsed, unfocused laser used for the excitation. Auxiliary fields grow in the traveling-wave, transient response of the atomic medium to the two-photon pumping field. A transient inversion exists between the excited ^3P and the lower-lying, dipole-coupled, ^3S level of atomic O. Thus one may expect amplified spontaneous emission (ASE) to grow along the propagation direction. The copropagating ASE radiation can affect the amount of (2+1)-photon ionization by deexciting the excited ^3P population to the ^3S, which rapidly decays to the ground manifold.

ASE is only one of the major concerns, however. Parametric wave growth involving four-wave mixing (FWM) transitions can occur in this system. Two of the photons in the FWM process come from the pumping field, and the other two from downward transitions through an intermediate level. Competition between ASE and FWM in the (2+1)-photon excitation process has been studied by Boyd, Malcuit, Gauthier, and Rzaszewski[2] (BMGR) in the steady-state approximation, with a perturbational treatment of the medium response to the two-photon-resonant applied pump field. Whereas ASE growth can only lessen the (2+1)-photon ionization efficiency by saturating the excited ^3P-^3S transition, FWM growth would appear to suppress the (2+1)-photon process *completely* under the right circumstances.[2]

The objective of this work is to analyze the time-and-distance-dependent growth of auxiliary fields in the (2+1)-photon excitation scheme for atomic O. Here the work differs from BMGR in that the system is time dependent instead of steady state, and that the exciting field is treated as a strong field for which one must use a nonperturbative solution for the density matrix. Because of these less stringent assumptions, I cannot use the steady-state saturating wave solution as found by BMGR.[2]

Physical considerations allow a reasonable approximation to the O system to consist of three levels (each degenerate) and the ionization continuum, and three radiation fields with the near-resonant condition, $\omega_2+\omega_3 \simeq 2\omega_1$. This notation is clarified in Fig. 1. The application to the high atmosphere allows a study of a collisionless medium in which natural radiative decay and the Doppler effect are the only important broadening effects.

The paper is organized as follows. Section II gives the basic Maxwell-Bloch equations with multiphoton couplings. Section III analyzes the equations for weak auxiliary field growth in the medium as it responds to the strong multiphoton pump field. Section IV presents the numerical solutions to the Bloch-Maxwell equations for strong coupling among all waves and the medium, and Sec. V is a discussion.

II. BASIC THEORY

Because part of this work contains basic analytical expressions and also because the phases are treated some-

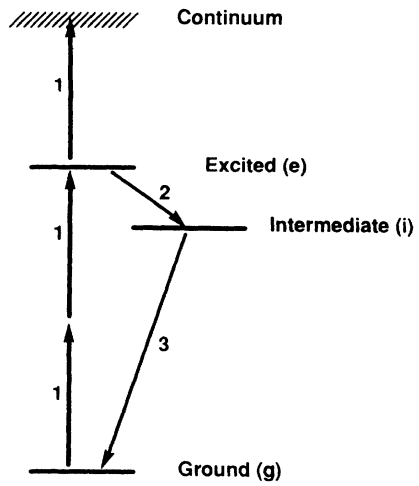

FIG. 1. One ladder of the coupling used to describe (2+1)-photon ionization of O and parametric growth. g denotes a $2p^4\,{}^3P_{2M}$ ground state, e denotes a $({}^4S^0)3p\,{}^3P_{2M}$ state, and i denotes a $({}^4S^0)3s\,{}^3S_{1M}$ state. The fields are plane polarized on a common axis. ASE growth involves transitions at ω_2 from e to i. FWM involves growth at ω_2 and ω_3 coupled to the two-photon transition from g to e.

what unconventionally, I outline the derivation of the effective Maxwell-Bloch equations for the system. Following the Icsevgi and Lamb procedure,[3] the real electric ($E^{\rm re}$) and induced polarization ($P^{\rm re}$) fields are decomposed as

$$F^{\rm re}=\sum_l F_l^{\rm re},\quad F_l^{\rm re}=\frac{1}{2}\sum_{\pm}F_l^{\pm}e^{\pm i\omega_l\tau} \tag{1}$$

where F denotes E or P, and $F^+=F$, $F^-=F^*$ (complex conjugate). ω_l are a set of carrier frequencies. The Maxwell equation in one dimension,

$$\left[-\frac{\partial^2}{\partial z^2}+\frac{\partial^2}{c^2\partial t^2}\right]E^{\rm re}=-\mu_0\frac{\partial^2}{\partial t^2}P^{\rm re}\ , \tag{2}$$

reduces in the slowly varying envelope approximation to the set of equations,

$$\frac{\partial}{\partial z'}E_l=\frac{-ik_l}{2\epsilon_0}P_l\ . \tag{3}$$

Coordinate transformations have been used to express relations in the retarded frame (τ and z'):

$$\begin{aligned} &z'=z,\quad \tau=t-z/c\ ,\\ &\frac{\partial}{\partial z'}=\frac{\partial}{\partial z}+\frac{\partial}{c\,\partial t},\quad \frac{\partial}{\partial\tau}=\frac{\partial}{\partial t}\ . \end{aligned} \tag{4}$$

Let $\underline{D}$ denote the constant, atomic, electric dipole matrix, then the optical Bloch equation for the response of the medium to the field is

$$\dot{\underline{\rho}}(v)=(i/\hbar)E^{\rm re}(v)[e^{i\underline{\omega}\tau}\underline{D}e^{-i\underline{\omega}\tau},\underline{\rho}(v)]-\tfrac{1}{2}\{\underline{\gamma},\underline{\rho}(v)\}+\underline{\Lambda}\ . \tag{5}$$

The overdot denotes $\partial/\partial t$ or $\partial/\partial\tau$, and I have used the retarded time variable for the transformation to the rotating atomic frame. Braces denote the anticommutator. The argument v is written explicitly in Eq. (5) to show that this Bloch equation applied to atoms moving with velocity v along the propagation direction. The Doppler effect is included in the fields as an apparent frequency. The diagonal $\underline{\omega}$ matrix is defined from atomic eigenvalues, $\omega_{ii}=(W_i-W_0)/\hbar$. The diagonal $\underline{\gamma}$ matrix contains the spontaneous atomic decay rates (collisional damping is unimportant in the application), and the diagonal source matrix $\underline{\Lambda}$ is due to these decays and is a function of the populations (diagonal of $\underline{\rho}$). The medium polarization (dipole density), which acts as the Maxwell equation source term in Eq. (2), is given by

$$P^{\rm re}=\int dv\ {\rm Tr}\{\exp[i\underline{\omega}(v)\tau]\underline{D}\exp[-i\underline{\omega}(v)\tau]\underline{\rho}\}\ . \tag{6}$$

The atomic frequencies in Eq. (6) are corrected by a factor $\omega_{ii}(v)=\omega_{ii}(1+v/c)$ to account for the atomic velocity. This completes the outline of the construction of the close-coupled Maxwell-Bloch equations.[3]

This general description is now specialized to a field which is two-photon resonant with an excited level and also coupled to the ionization continuum. Other fields are assumed to be nearly resonant with the intermediate level as shown in Fig. 1. Note that no restrictions have been made as to field strengths or exact resonance of the carrier frequencies to the atom. Neither has it been assumed that $2\omega_1=\omega_2+\omega_3$ in order to remove certain explicit time dependencies from the rotating-wave Bloch equation. The factorization of the carrier waves from the amplitudes as done here allows complete freedom in the time and space (i.e., frequency and wave number when transformed) growth of all the fields. In order to do calculations with this Bloch equation, one must develop an effective Bloch equation for the two-photon couplings which eliminates all of the weakly coupled and highly nonresonant intermediate states driven by the strong pump field at ω_1. This is done next.

The procedure of iterating the Bloch equation and evaluating the off-resonance couplings asymptotically in order to obtain the effective two-photon couplings is well known.[4] Equation (5) is first converted to a Volterra equation, including the $\underline{\gamma}$ in the kernel. $E^{\rm re}$ consists of a sum of three fields, with frequencies near ω_1, ω_2, and ω_3. With $E^{\rm re}$ so decomposed, $\underline{\rho}$ is iterated once by substitution into the integral containing $E_1^{\rm re}$. Only slowly varying terms are retained by utilizing asymptotic approximations based on

$$\int_{\infty}^{\tau}d\tau' f(\tau')e^{-\Gamma(\tau-\tau')}e^{i\delta\tau'}\underset{\delta\to\infty}{\sim}f(\tau)e^{i\delta\tau}/(i\delta+\Gamma)\ .$$

The approximated integral equation can be converted back to an effective Bloch equation [where $\underline{H}=\underline{H}(v)$ is a Rabi frequency, including phase],

$$\dot{\underline{\rho}}=(i/2)[\underline{H},\underline{\rho}]-(\tfrac{1}{2})\{\underline{\gamma},\underline{\rho}\}+\underline{\Lambda}\ . \tag{7}$$

The coupling elements of $\underline{H}$ are evaluated in terms of atomic parameters, with i, g, and e denoting intermediate, ground, and excited states, to be

$$H_{ig}=\frac{1}{\hbar}D_{ig}E_3^{*}e^{i\Delta_{ig}^{3}\tau}\ ,$$
$$H_{ei}=\frac{1}{\hbar}D_{ei}E_2^{*}e^{i\Delta_{ei}^{2}\tau}\ , \tag{8}$$

$$H_{gg}=-\frac{1}{2\hbar}|E_1|^2\sum_{\pm}M_{gg}(\omega_g\pm\omega_1)\ , \tag{9}$$
$$H_{ee}=-\frac{1}{2\hbar}|E_1|^2\mathrm{Re}\left[\sum_{\pm}M_{ee}(\omega_e\pm\omega_1+i\epsilon)\right]\ ,$$

$$H_{eg}=-\frac{1}{2\hbar}(E_1^{*})^2M_{eg}(\omega_g+\omega_1)e^{i\Delta_{eg}^{11}\tau}\ , \tag{10}$$
$$H_{ge}=-\frac{1}{2\hbar}(E_1)^2M_{ge}(\omega_e-\omega_1)e^{-i\Delta_{eg}^{11}\tau}\ ,$$

$$M_{ij}(z)=\frac{1}{\hbar}\sum_{k}\frac{D_{ik}D_{kj}}{z-\omega_k}\ , \tag{11}$$

$$\Delta_{ij}^{l}=\Delta_{ij}^{l}(v)=\omega_{ij}-\omega_l(v)\ , \tag{12}$$
$$\omega_l(v)=\omega_l(1-v/c)\ ,$$

$$\omega_{ij}=\omega_{ii}-\omega_{jj}\ , \tag{13}$$

$$\Delta_{ij}^{ll}=\Delta_{ij}^{ll}(v)=\omega_{ij}-2\omega_l(v)\ . \tag{14}$$

Generally $\underline{H}=\underline{H}^{\dagger}$, except for an insignificant difference in the pair of Eq. (10). Equation (9) contains the dynamic ac stark shift due to E_1. An ionization rate out of e is included in $\underline{\gamma}$. The ionization rate is

$$\gamma_e^{I}=\frac{1}{2\hbar}|E_1|^2\mathrm{Im}\left[-\sum_{\pm}M_{ee}(\omega_e\pm\omega_1+i\epsilon)\right]\ . \tag{15}$$

The carrier frequencies of the fields are Doppler corrected by $\omega_l(v)=\omega_l(1-v/c)$, as indicated in Eq. (12).

Equation (7) is integrated numerically for the ionization dynamics of an atom subject to the three fields. The coupling parameters involving the M_{ij} for atomic oxygen are obtained from the work of DLM.[1] These will be given in a later section.

The response of the medium to the fields in turn affects the fields' propagation. By equating P^{re} in decomposed form in Eq. (1) to the expectation value in Eq. (6) and extracting the proper slowly varying terms, one finds

$$P_2=2\int dv\ D_{ei}\rho_{ie}(v)e^{i\Delta_{ei}^{2}(v)\tau}\ ,$$
$$P_3=2\int dv\ D_{ig}\rho_{gi}(v)e^{i\Delta_{ig}^{3}(v)\tau}\ . \tag{16}$$

When combined with Eq. (13), these determine the propagation of the dipole-coupled (single-photon resonant) fields E_2 and E_3. The induced medium polarization at frequency ω_1, which determines the absorption of the two-photon field as well as its phase shift, can be derived, but the extinction and refraction of E_1 are totally negligible over the lengths of interest for analysis of the growth of parametric waves E_2 and E_3. I drop P_1 from consideration.

III. EARLY GROWTH OF PARAMETRIC WAVES

In order to ionize a substantial fraction of the atoms, E_1 must be strong, with intensity on the order of GW/cm^2. At the beginning of the channel of ionization, only E_1 is present; fields E_2 and E_3 generate from spontaneous emission and FWM along the propagation direction. Because of the weak two-photon coupling and small ionization cross section from the excited level e, field E_1 remains essentially unperturbed throughout the channel length independent of the strength of E_2 and E_3 and the atomic response. In the early growth region, I can obtain the evolution of E_2 and E_3 as perturbations upon the strong-coupled, zeroth-order response of the density matrix of the medium to E_1.

To begin this construction of the early parametric growth, Eq. (7) is converted to Volterra form,

$$\underline{\rho}(\tau)=\underline{\rho}(-\infty)+(i/2)\int_{-\infty}^{\tau}d\tau'\exp\left[-\frac{1}{2}\int_{\tau'}^{\tau}\underline{\gamma}\right]\times[\underline{H},\underline{\rho}]\exp\left[-\frac{1}{2}\int_{\tau'}^{\tau}\underline{\gamma}\right]+\int_{-\infty}^{\tau}d\tau'\underline{\Lambda}\ . \tag{17}$$

The velocity dependence is implicit here as it is in Eq. (7). The effective coupling matrix $\underline{H}$ is written as a zeroth-order part $\underline{H}^0$ depending on E_1 and a first-order part $\underline{H}^1$ depending on E_2 and E_3. $\underline{H}^0$ contains coupling between g and e. Assume that $\underline{\rho}^0$ is the known solution to Eq. (17) with $\underline{H}$ replaced by $\underline{H}^0$. The first-order correction to $\underline{\rho}^0$ due to $\underline{H}^1$ is found to be

$$\underline{\rho}^1=(i/2)\int_{-\infty}^{\tau}d\tau'\exp(-\tfrac{1}{2}\int_{\tau'}^{\tau}\underline{\gamma})\times[\underline{H}^1,\underline{\rho}^0]\exp(-\tfrac{1}{2}\int_{\tau'}^{\tau}\underline{\gamma})\ . \tag{18}$$

Only the off-diagonal parts of $\underline{\rho}^1$ are needed and written in Eq. (18). When Eq. (18) (the induced medium coherences due to E_2 and E_3) is combined with the field-growth Eq. (3), I have a description of the growth of fields E_2 and E_3 in the presence of the strong field E_1.

By a straightforward set of algebraic manipulations, Eq. (18) is converted into a pair of field-growth equations for E_2 and E_3. First, $\underline{H}^1$ is replaced by the fields as given in Eq. (8); second, Eq. (18) is written explicitly for matrix elements ρ_{ei}^1 and ρ_{ig}^1, and their conjugates; third, Eq. (16) is used to relate these to the polarization amplitudes; and fourth, the polarizations are substituted into the field-amplitude growth Eq. (3). This results in a pair of coupled integrodifferential equations for E_2 and E_3:

$$\frac{\partial E_2}{\partial z'}=(k_2/2\epsilon_0\hbar)\int_{-\infty}^{\infty}dv\ e^{i\Delta_{ei}^{2}\tau}D_{ei}\int_{-\infty}^{\tau}d\tau'\exp(-\int_{\tau'}^{\tau}\Gamma_{ie})(E_3^{*}e^{i\Delta_{ig}^{3}\tau'}D_{ig}\rho_{ge}^{0}+E_2e^{-i\Delta_{ei}^{2}\tau'}D_{ie}\rho_{ee}^{0})\ , \tag{19}$$

$$\frac{\partial E_3}{\partial z'}=-(k_3/2\epsilon_0\hbar)\int_{-\infty}^{\infty}dv\ e^{i\Delta_{ig}^{3}\tau}D_{ig}\int_{-\infty}^{\tau}d\tau'\exp(-\int_{\tau'}^{\tau}\Gamma_{gi})(E_2^{*}e^{i\Delta_{ei}^{2}\tau'}D_{ei}\rho_{ge}^{0}+E_3e^{-i\Delta_{ig}^{3}\tau'}D_{gi}\rho_{gg}^{0})\ . \tag{20}$$

In Eqs. (19) and (20), the Δ_{ij}^{I} are functions of atomic velocity, as well as is the zeroth-order solution $\underline{\rho}^0$. $\Gamma_{ij}=(\gamma_i+\gamma_j)/2$ has been introduced also. Equations (19) and (20) can be simplified if the Doppler effect can be neglected compared to other "broadening" effects in the system. For heuristic reasons, I assume this is true in the early-growth analysis. With this understanding, define

$$y_2=E_2e^{-i\Delta_{ei}^2\tau}, \qquad y_3=E_3e^{-i\Delta_{ig}^3\tau}, \tag{21}$$

which is equivalent to a specification of the carrier frequencies in terms of the atomic transition frequencies. It should be noted that "off-resonance" growth of the fields will appear as highly oscillatory phases in the factored amplitude functions with this specification of the carrier waves. Equations (19) and (20) may now be written as a pair of coupled partial differential equations,

$$\left[\underline{1}\frac{\partial}{\partial\tau}+\underline{\Gamma}(\tau)\right]\frac{\partial}{\partial z'}\underline{y}(z',\tau)=\underline{M}(\tau)\underline{y}(z',\tau), \tag{22}$$

where

$$\underline{y}=\begin{bmatrix}y_2\\ y_3^*\end{bmatrix}, \quad \underline{\Gamma}=\begin{bmatrix}\Gamma_{ei} & 0\\ 0 & \Gamma_{ig}\end{bmatrix}, \tag{23}$$

and

$$\underline{M}=(1/2\epsilon_0\hbar)\begin{bmatrix}k_2 & 0\\ 0 & -k_3\end{bmatrix}\times\begin{bmatrix}|D_{ie}|^2\rho_{ee}^0 & D_{ei}D_{ig}\rho_{ge}^0\\ D_{gi}D_{ie}\rho_{eg}^0 & |D_{ig}|^2\rho_{gg}^0\end{bmatrix}. \tag{24}$$

The retarded time dependence of $\underline{M}$ is contained in $\underline{\rho}^0$, that of $\underline{\Gamma}$ in the ionization rate of e in γ_e^I. Equation (22) is the primary result of this analysis for an evolution equation describing the early growth of the parametric fields.

A. Solutions of parametric growth

If the (2+1)-photon excitation dynamics are such that the ρ_{eg}^0 coherence density is small, then Eq. (22) is approximately decoupled and the evolution of E_2 and E_3 (i.e., $\underline{y}$) may be written down exactly,[3]

$$y_i(z',\tau)=\int_{-\infty}^{\tau}d\tau' I_0\left[2\left[z'\int_{\tau'}^{\tau}M_{ii}(\tau'')d\tau''\right]^{1/2}\right]\times\frac{\partial}{\partial\tau'}\left[y_i(0,\tau')\exp\left[-\int_{\tau'}^{\tau}\Gamma_{ii}\right]\right]. \tag{25}$$

The index i denotes either field 2, in which case ρ_{ee}^0 and Γ_{ei} appear, or field 3, in which the case ρ_{gg}^0 and Γ_{ig} appear on the right-hand side (RHS). I_0 is the modified Bessel function. If the argument of I_0 is imaginary due to negative M_{ii}, I_0 becomes J_0. The solution as presented in Eq. (25) describes the small signal amplification or extinction of waves E_2 and E_3 as they evolve in a traveling-wave medium consisting mainly of *population* response to the (2+1)-photon pump field E_1. It can be seen that field E_2 is amplified (ASE) and E_3 absorbed. This is the case when the atomic coherence is rapidly destroyed by collisions.

In general it is incorrect to assume that $\underline{\rho}^0$ is nearly diagonal. In the application of interest here, namely, O in the high atmosphere, collisions are almost nonexistent. The (2+1)-photon excitation and ionization process creates a high degree of coherence in the medium, with ionization to the continuum being the major source of coherence damping in the g to e transition. In this situation the zeroth-order density matrix can be factored into the outer product of vector solutions to the effective Schrodinger equation:

$$\underline{\rho}^0=\underline{c}^0\underline{c}^{0\dagger}, \tag{26}$$

where

$$\dot{\underline{c}}^{\,0}=(i/2)\underline{H}^0\underline{c}^0-\tfrac{1}{2}\underline{\gamma}\underline{c}^0. \tag{27}$$

The radiative source term is dropped, as the radiative decay from level e is insignificant compared to ionization. Equation (26) forces an immediate connection of populations and coherence density, $|\rho_{eg}|^2=\rho_{ee}\rho_{gg}$. The decomposability of $\underline{\rho}^0$ leads to a decomposition of $\underline{M}$ in Eq. (24):

$$\underline{M}=(1/2\epsilon_0\hbar)\begin{bmatrix}k_2 & 0\\ 0 & -k_3\end{bmatrix}\underline{v}\,\underline{v}^{\dagger}, \quad \underline{v}=\begin{bmatrix}D_{ei}c_e^*\\ D_{gi}c_g^*\end{bmatrix}. \tag{28}$$

$\underline{M}$ is singular with one zero eigenvalue, say, $\lambda_-=0$. The nonzero eigenvalue is found to be

$$\lambda_+=\lambda_+(\tau)=(1/2\epsilon_0\hbar)(k_2|D_{ie}|^2\rho_{ee}^0-k_3|D_{ig}|^2\rho_{gg}^0). \tag{29}$$

This eigenvalue is of importance because the coupled solution to Eq. (22) may be approximated as the adiabatic solution of the diagonalized equation [$\underline{S}=\underline{S}(\tau)$]:

$$\underline{y}=\underline{S}\,\underline{z}, \quad \underline{S}^{-1}\underline{M}\,\underline{S}=\underline{\lambda}=\begin{bmatrix}\lambda_+ & 0\\ 0 & \lambda_-\end{bmatrix}, \tag{30}$$

$$\underline{S}=\begin{bmatrix}k_2v_1 & v_2^*\\ -k_3v_2 & -v_1^*\end{bmatrix}, \quad \underline{S}^{-1}=D^{-1}\begin{bmatrix}-v_1^* & -v_2^*\\ k_3v_2 & k_2v_1\end{bmatrix}, \tag{31}$$

$$D=-k_2|v_1|^2+k_3|v_2|^2=-2\epsilon_0\hbar\lambda_+, \tag{32}$$

where $v_1=D_{ei}c_e^*$ and $v_2=D_{gi}c_g^*$ as appear in Eq. (28). The approximate solutions obey

$$\left[\frac{\partial}{\partial\tau}+\Gamma\right]\frac{\partial}{\partial z'}z_{\pm}=\lambda_{\pm}z_{\pm}, \tag{33}$$

where the adiabatic coupling term involving $\underline{S}$ has been dropped, and $\underline{\Gamma}$ has been approximated by the scalar $\Gamma=\gamma_i/2$, where γ_i is the constant rapid decay rate of *intermediate* level i. The explicit solutions are

$$z_-(z',\tau)=z_-(0,\tau), \tag{34}$$

$$z_+(z',\tau)=\int_{-\infty}^{\tau}d\tau' I_0\left[2\left[z'\int_{\tau'}^{\tau}d\tau''\lambda_+(\tau'')\right]^{1/2}\right]\times\frac{\partial}{\partial\tau'}[z_+(0,\tau')e^{-\Gamma(\tau-\tau')}]. \tag{35}$$

Because of the zero eigenvalue, the z_- solution does not evolve. The solution for z_+ in Eq. (35) is much the same as Eq. (25). These solutions are discussed below.

Although the work here concerns strong time dependent effects, it is worth mentioning that Eq. (22) as well as Eq. (33) can be solved for the Fourier components of $\exp(i\omega\tau)$ assuming that $\underline{M}$ and $\underline{\Gamma}$ are constant. This leads to an examination of the eigenvalues of $(i\omega\underline{1}+\underline{\Gamma})^{-1}\underline{M}$, namely, $\lambda_\pm$ which are now constant, and contain wave numbers modified by the replacement of k_i by $k_i/(i\omega+\Gamma_{ii})$ in Eq. (29). The spatial growth is thus seen to be Lorentzian in frequency dependence. The adiabatic approximation is not valid if strong Rabi oscillations occur on the two-photon excitation. Likewise it must be modified to accommodate a large detuning of ω_1.

B. Discussion of solutions

The early evolution of parametric fields E_2 and E_3 along the traveling-wave excitation channel can be understood in terms of the adiabatic eigenvalue λ_+. First, one must determine how λ_+ controls the evolution of solutions to the equation,[3]

$$\frac{\partial^2}{\partial\tau\,\partial z'}Z(z',\tau)=\lambda_+(\tau)Z(z',\tau)\ , \tag{36}$$

where the damping term of Eq. (22) or Eq. (33) has been dropped. The exact solution is

$$Z(z',\tau)=\int_{-\infty}^{\tau}d\tau' I_0\left[2\left[z'\int_{\tau'}^{\tau}\lambda_+\right]^{1/2}\right]\times\frac{\partial}{\partial\tau'}Z(0,\tau')\ , \tag{37}$$

or

$$Z(z',\tau)=\int_{-\infty}^{\tau}d\tau' J_0\left[2\left[-z'\int_{\tau'}^{\tau}\lambda_+\right]^{1/2}\right]\times\frac{\partial}{\partial\tau'}Z(0,\tau') \tag{38}$$

for negative regions of the integral in the argument of the Bessel function. Analysis shows that positive λ_+ results in growth, and negative λ_+ in absorption. These solutions may be shown to exhibit considerable pulse dispersion (drag), which will show up markedly in the numerical solutions to be presented later. Simple analytical approximations and/or assumptions may be made on the RHS of Eq. (37) or (38) in order to explore the evolution of the solution. It should be noted that the damping terms in $\underline{\Gamma}$ are not necessary for growth or absorption of the coupled solutions contained in Z. This is not so when one solves Eqs. (19) and (20), or Eq. (22), in the steady-state approximation by the substitution of steady waves $[\exp(i\omega\tau)]$ for the fields. In that limit the damping term is crucial for coupled-wave growth or loss. This would appear contradictory, but the Fourier width of the time-dependent pulse apparently can substitute for the medium damping.

Thus, I conclude that the approximate threshold for parametric growth is conditional on the real quantity λ_+ being positive, which depends on the weighted population difference between the two-photon-pumped level e and the ground level g as given in Eq. (29). One expects a sufficiently strong E_1 field to cause the retarded time dependence of λ_+ to rise from the negative value associated with the ground-level density to a possibly positive value depending on the populations of levels e and g, and the dipole couplings to state i. The maximum value attained by ρ_{ee} during the pump pulse is roughly determined by the balance between two-photon pumping rate and ionization rate out of e. This indicates the very atom- and transition-specific nature of the growth condition.

It is of interest to know the energy balance of the growing fields. If $\underline{\rho}^0$ were diagonal, that is consisting of populations, then Eq. (25) shows that E_2 and E_3 evolve independently. The only growing field is ASE in E_2. However, the coherence of g and e, as shown by ρ^0_{eg}, and the outer product decomposition of $\underline{\rho}^0$ in Eq. (26), forces the growing solution to be a coupled combination of E_2 and E_3. The mixing of E_2 and E_3 is given by the adiabatic approximation in Eqs. (30)–(35). I find

$$\begin{aligned} y_2&=k_2D_{ei}c_e^*z_+\ ,\\ y_3^*&=-k_3D_{gi}c_g^*z_+\ , \end{aligned} \tag{39}$$

or

$$\begin{aligned} |E_2|^2&=k_2^2|D_{ei}|^2\rho^0_{ee}|z_+|^2\ ,\\ |E_3|^2&=k_3^2|D_{gi}|^2\rho^0_{gg}|z_+|^2\ . \end{aligned} \tag{40}$$

Thus it is seen in Eq. (40) that the fields are not required to grow in any particular photon number ratio in the early growth region. Later, in Section IV D, the numerical solutions in the strong coupling region will show that the fields evolve into a growing combination of waves that does have equal photon numbers in ω_2 and ω_3. There is, however, a connection of the photon numbers to the growth eigenvalue; from Eqs. (29) and (40) one finds that $(I_l=ce_0|E_l|^2/2)$

$$I_2/\hbar\omega_2-I_3/\hbar\omega_3=\epsilon_0^2|z_+|^2\lambda_+\ . \tag{41}$$

Thus a positive λ_+, which results in a growing z_+, causes I_2 to grow faster than I_3 in photon number. This could be regarded as an ASE component in the solution.

This raises the question as to why the equations do not contain distinct positive eigenvalues for ASE and FWM growth. The structure of $\underline{\rho}^0$ determines this. The eigenvalues of $\underline{M}$ are

$$\lambda_\pm=(1/4\epsilon_0\hbar)\{T_2-T_3\pm[T_2^2+T_3^2-2T_2T_3(2f-1)]^{1/2}\}\ , \tag{42}$$

where

$$\begin{aligned} T_2&=k_2|D_{ie}|^2\rho_{ee}\ ,\\ T_3&=k_3|D_{ig}|^2\rho_{gg}\ , \end{aligned} \tag{43}$$

and I have set

$$|\rho^0_{eg}|^2=f\rho^0_{gg}\rho^0_{ee}\ . \tag{44}$$

The positive number f ranges from zero to one, and mea-

sures the amount of coherency in the (2+1)-photon pumping process. The coherent case ($f=1$, discussed above) has eigenvalues

$$\lambda_+=(T_2-T_3)/2\epsilon_0\hbar,\quad \lambda_-=0\ , \tag{45}$$

and the incoherent case ($f=0$, ASE and absorption) has

$$\lambda_+=T_2/2\epsilon_0\hbar,\quad \lambda_-=-T_3/2\epsilon_0\hbar\ . \tag{46}$$

Analysis shows that, for $0\le f\le 1$, at most one of the eigenvalues can be positive. Consequently I do *not* see independent early growth of FWM and ASE. The growing waves are a close-coupled mixture of the two frequencies and are inseparable insofar as the adiabatic approximation to Eq. (22), as given in Eqs. (30)–(35), is a valid solution. An upper bound on the eigenvalues is $T_2/2\epsilon_0\hbar$.

In the collisionless environment of the upper atmosphere that is being studied here, the only mechanisms that lower the coherency of ρ^0 (drive f to a small value) are a noisy E_1 and a large Doppler effect. The detuning of ω_1 from the two-photon transition and the ac Stark effect can play an analogous role in affecting the growth of the parametric fields.

IV. NUMERICAL SOLUTIONS FOR ATOMIC OXYGEN

In this section I apply the Maxwell-Bloch description to a simplified model of the (2+1)-photon ionization of O and growth of parametric waves. The early-growth analysis of Sec. III was useful for deriving the threshold condition, $\lambda_+>0$, but it did not address gain saturation effects, laser detuning, or the Doppler effect. This section will explore these effects.

A. Atomic and laser data for the oxygen transitions

Consider a collisionless low-density gas of O atoms subjected to an intense pulsed laser field E_1 with wavelength λ_1 around 226 nm. The pulse amplitude is assumed to be a transform-limited, plane-polarized, temporal and spatial Gaussian with a nominal intensity FWHM of 0.3 ns. With LS-coupled atomic states quantized on the electric vector direction, the laser field couples states JM_J to $J'M_J$, remaining diagonal in M_J. Spontaneous emission from excited levels weakly couples M_J to M_J'. The 226-nm laser is tuned to be two-photon resonant with the transition from the ground (g) $J=2$ level of the ground ^3P_J manifold to the $J=2$ level of the first excited (e) ^3P_J manifold. The e states are pumped to the structureless ionization continuum by the same laser. There are five M_J ladders involved in the pumping, each resembling the ladder of Fig. 1. In addition to the pump laser E_1, I wish to allow for fields E_2 and E_3 arising from growth of spontaneously emitted radiation. These fields couple to the intermediate (i) $^3S_1$ level consisting of three states. E_2 and E_3 are assumed plane polarized on the direction of E_1. In order to reduce the dimensionality of the Bloch equations, the weakly coupled $M_J=\pm 2$ ladder is neglected in the (2+1)-photon pumping, leaving the $M_J=0,\pm 1$ ladders, each of three levels, coupled by the three fields and spontaneous emission. The $M_J=\pm 1$ ladders are equivalent, which leaves a pair of weakly coupled 3×3 density matrices. An accounting of the Doppler effects expands the Bloch system into an array of density matrices which are solved independently for each velocity bin and subsequently summed to give the medium response to the fields.[3]

Most of the atomic data for (2+1)-photon ionization of O have been calculated by quantum defect theory by DLM.[1] One needs the ac Stark shifts, the effective two-photon couplings, and the ionization rates for the g^3P_{2M} to e^3P_{2M} transitions. DLM report their results in terms of rates per W/cm^2. Writing the ionization rate in Eq. (15) as

$$\gamma_e^I=\sigma_{JM}^{\rm ion}(c\epsilon_0|E_1|^2/2\hbar\omega_1)\ , \tag{47}$$

the DLM values become

$$\begin{aligned}&\sigma_{20}^{\rm ion}=7.15\times 10^{-19}\ {\rm cm}^2\ ,\\ &\sigma_{2\pm 1}^{\rm ion}=5.65\times 10^{-19}\ {\rm cm}^2\ ,\\ &\sigma_{2\pm 2}^{\rm ion}=1.13\times 10^{-19}\ {\rm cm}^2\ .\end{aligned} \tag{48}$$

These ionization cross sections compare favorably with literature values.[5,6] The ac Stark terms of Eq. (9) are proportional to intensity. One identifies my H_{ii} in Eq. (9) as $-2S_i$, where the $S_i=S_{iJM}$ are level shifts calculated by DLM to be, in rad/s per W/cm^2,

$$\begin{aligned}&S_{g20}=-0.410,\quad S_{g2\pm 1}=-0.321\ ,\\ &S_{e20}=6.24,\quad S_{e2\pm 1}=6.37\ .\end{aligned} \tag{49}$$

The effective two-photon coupling in Eq. (10) can be expressed in terms of intensity if the field amplitude is real. Identification of a Rabi rate as

$$\Omega_{ge}^M=-H_{ge}e^{i\Delta_{eg}^{11}\tau} \tag{50}$$

from Eqs. (7) and (10) is straightforward. DLM report, in rad/s per W/cm^2, for the $J=2$ to $J=2$ transitions,

$$\begin{aligned}&\Omega_{ge}^0=-3.84\ ,\\ &\Omega_{ge}^{\pm 1}=-3.18\ ,\\ &\Omega_{ge}^{\pm 2}=-1.21\ .\end{aligned} \tag{51}$$

The $M_J=\pm 2$ value is included here and in Eq. (48) to show that its 2 ± 1 pumping efficiency is small. The square of the Rabi rate is a good measure of the pumping to e, and this shows that my neglect of the $M_J=\pm 2$ ladder is less than a 10% error in the absence of saturation of the $M_J=\pm 2$ ladders.

The data for the dipole-coupled e to i and i to g transitions consists of the D_{ei}^M and D_{ig}^M matrix elements of Eq. (8). These can be evaluated from oscillator strengths,[7] using observed values.[8,9] For the states at hand, in units of 10^{-30} Cm, I find

$$\begin{aligned}&D_{ei}^0=-20.0,\quad D_{ei}^{\pm 1}=-17.3\ ,\\ &D_{ig}^0=3.39,\quad D_{ig}^{\pm 1}=2.93\ .\end{aligned} \tag{52}$$

The spontaneous (natural) decay rates[8,9] are

$$\gamma_i^N = 0.67 \text{ ns}^{-1} ,$$
$$\gamma_e^N = 0.028 \text{ ns}^{-1} . \quad (53)$$

The repopulation of lower levels due to spontaneous decay is included here for completeness. In terms of the J to J' rate $\gamma_{JJ'}$, I have derived the JM_J to $J'M_J'$ rate to be, using 3-J symbols,[7]

$$\gamma_{JM_JJ'M_J'} = \gamma_{JJ'}(2J+1) \sum_{m=-1,0,1} \begin{pmatrix} J & 1 & J' \\ -M_J & m & M_J' \end{pmatrix}^2 . \quad (54)$$

One notes from Eq. (53) that level e decays slowly to i, which in turn decays rapidly to all levels in the ground manifold. The specific decay rate of $i\ ^3S_1$ to $g\ ^3P_2$ is 0.37 ns^{-1}.[8]

A further comment should be made regarding the rather closely spaced excited ^3P_J levels. The $J=2$ and $J=0$ separation is 0.16 cm^{-1} (5 GHz), which means that the Bloch equations should treat these as degenerate levels. The (2+1)-photon ionization studies of DLM treated all of the $e\ ^3P_J$ as degenerate. However, the $e\ ^3P_0$ coupling to the ground $^3P_2$ is fairly insignificant compared to the rest, so I ignore the $J=0$ level. The $^3P_1$ excited level is 0.54 cm^{-1} away from the $^3P_2$, which is sufficient separation not to be strongly pumped by the laser when it is tuned to the dominant fine structure line.

B. Numerical methods for the Maxwell-Bloch equation

I follow the basic outline of the Icsevgi-Lamb procedure,[3] but replace as much as possible of the integration by automatic error-control logic. The optical Bloch equations can be difficult to integrate in time if the fields are highly nonresonant. Because of this, a packaged Adams or Range-Kutta method with variable step control is used for the numerical solution of Eq. (7). In order to alleviate the frequent evaluation of the fields at closely spaced intervals when the time solution is difficult, I have used complex spline representations for all laser field envelopes and medium polarizations as a function of retarded time at each point in z. The splines allow an adequate interpolation from a fixed set of field values and time points. Typically a few hundred time points τ_i are adequate for the spline "basis." The Doppler integration over atomic velocities is reduced to a finite sum and tested for accuracy on each distinct problem. Typically the Doppler sum is evaluated to a few percent accuracy.

The propagation in z' (coordinate z) for the solution of Eq. (3) is basically a Heun method[10,11] with error analysis introduced on the "corrector" step. Let

$$\frac{\partial E(z',\tau)}{\partial z'} = f(z',\tau)$$

where f contains the medium polarization. The "predicted" field values are

$$E^P(z'+h,\tau) = E(z',\tau) + hf(z',\tau) ,$$

which are used to solve the Bloch equation at space point $z'+h$, determining a new set of medium responses and $f^P(z'+h,\tau)$. Propagation is done only on the spline points τ_i. The corrected field values are evaluated from

$$E(z'+h,\tau) = E(z',\tau) + \tfrac{1}{2}h[f(z',\tau) + f^P(z'+h,\tau)] .$$

The numerical error is monitored by comparing $E(z'+h,\tau)$ and $E^P(z'+h,\tau)$, with revision of h when a norm of the error is outside certain bounds. This explicit propagation scheme is low order and requires two Bloch solutions per space step. It has been quite successful on the (2+1)-photon ionization problem with parametric field growth.

C. (2+1)-photon ionization of atomic oxygen

The dynamics of the (2+1)-photon process have been explored by DLM (Ref. 1) in the limit of constant pump pulses of 5 and 10 ns, degenerate excited ^3P_J levels, and no Doppler effect. DLM include the excited $^3P_0$ and $^3P_1$ levels as well as the $M_J=\pm 2$ ladders in their calculations, which I do not. Allowing for this, my calculations agree semiquantitatively with their saturation and tuning curves, except that I do not reproduce the narrow subpeak structure in their Fig. 1(c) and at the peaks of their Fig. 2. These sharper structures are due to the small $M_J=\pm 2$ ionization cross section.[1] My ionization probabilities, shown in Fig. 2, saturate at precisely $\frac{3}{5}$ because the missing $M_J=\pm 2$ ladder omits $\frac{2}{5}$ of the initial $J=2$ ground level density. An examination of DLM's Figs. 1 and 2 shows the tendency of their results to saturate at 0.6 also. My calculations in Fig. 2 include the effect of excited ^3P_J degeneracy by increasing the two-photon Rabi rates to the geometric mean of the Rabi rates of the individual J components. This is somewhat appropriate as the assumption of degeneracy allows a new excited state to be defined as a superposition of the tabulated JM_J representation.[1]

In the (2+1)-photon ionization process, it is interesting

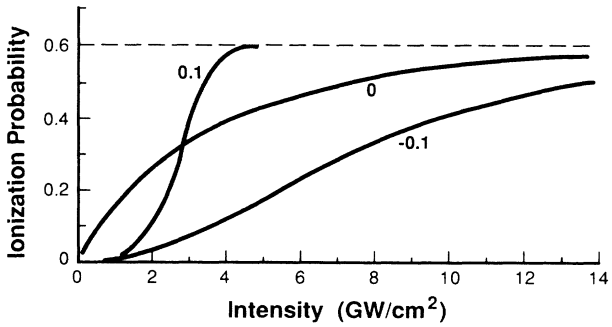

FIG. 2. Saturation of ionization probability from the ground $^3P_2$ level of O as a function of 226-nm laser intensity for a 5-ns constant pulse. The labels on the curves denote the detuning of the laser from the half transition energy in cm^{-1}. The $M_J=0,\pm 1$ ladders are included and the excited ^3P_J manifold is assumed degenerate as discussed in text. The asymmetry in the ± 0.1 saturation curves is due to the ac Stark shifts produced by the field.

to explore variations in laser intensity, pulse duration, and frequency, and in the Doppler effect of the medium. My investigation of parametric growth should also cover all these variations, but the amount of computation and data is too great, considering that this is a massive multistate, multifield, Doppler, distance- and time-dependent calculation. Some restrictions in scope are in order. The generation of the 226-nm radiation in our envisaged system suggests that the pump field will be a train of subnanosecond pulses with the cumulative effective resulting in a large ionization probability. Each pulse will ionize only 10% to 20% of the atoms. Moreover, the pulses may be continually displaced in frequency (chirped) so as to sweep over the Doppler profile. This suggests treating the pulses as incoherent with respect to one another and limiting the calculations to a fixed short pulse length.

Another savings is obtained by limiting the Bloch solution to a single M_J value. For a particular $J=2$ to $J'=2$

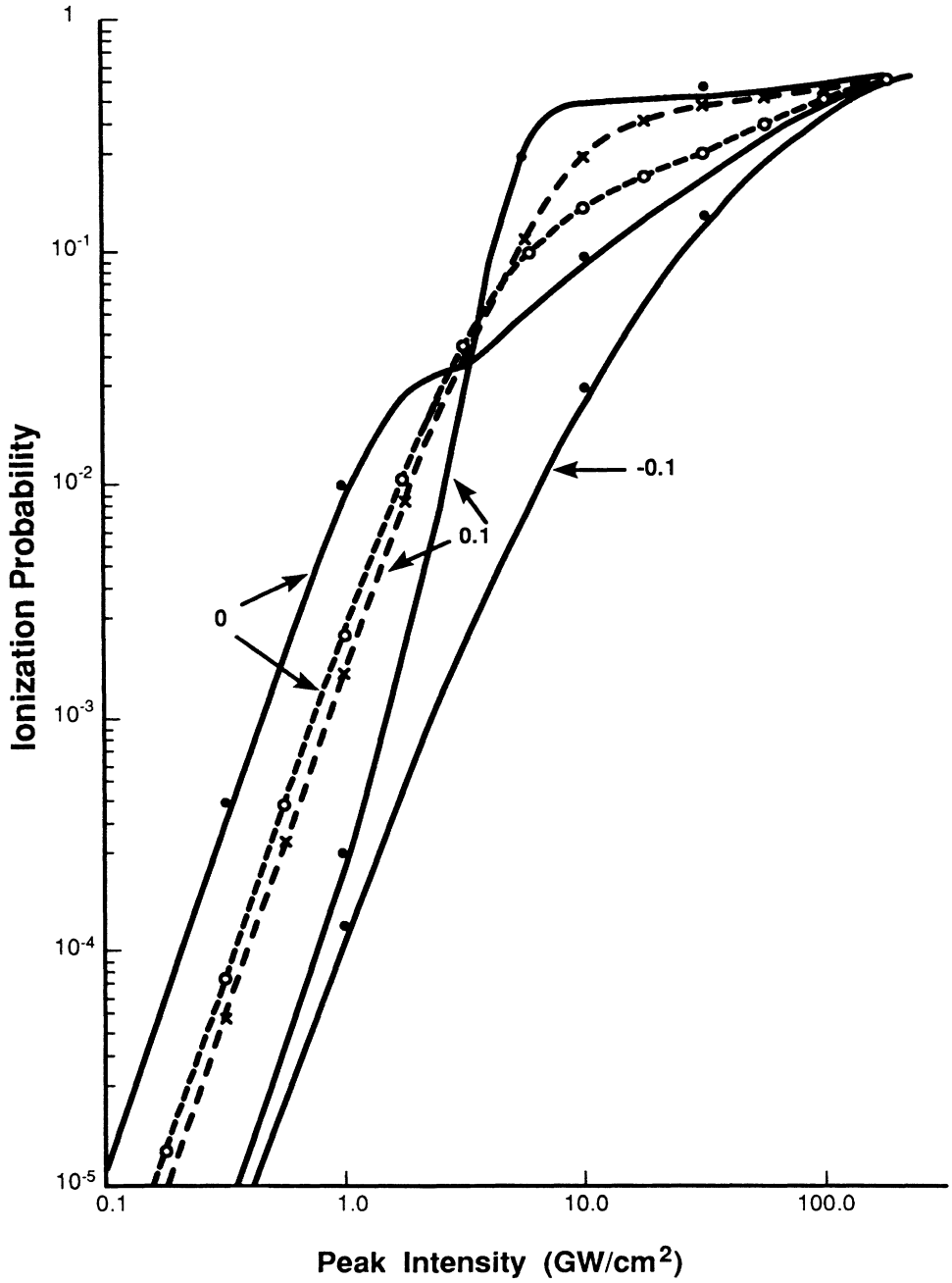

FIG. 3. Saturation of the ionization probability from the ground $^3P_2$ level of O as a function of 226-nm laser peak intensity for a 0.3-ns FWHM Gaussian pulse. The numeric labels on the curves denote the laser detuning in cm^{-1} from the half transition energy to the $^3P_2$ level. The solid curves are 0 K calculations based on the $M_J=1$ ladder through the e^3P_{21} excited state. The solid dots next to these curves are multiladder calculations based on e^3P_{2M}, $M=M_J=0,\pm1$. The curve designated as --○-- is a zero-detuned 800-K Doppler calculation and --×-- is a 0.1 cm^{-1} (laser) detuned 800-K Doppler case. 81 bins were used in the Doppler distribution.

transition and ionization of interest, one sees in Eqs. (48) and (51) that this is not a *major* error. It is also true that the dipole-coupled transitions are nearly the same for $M_J=0$ and $M_J=\pm 1$ as seen in Eq. (52). To do the Maxwell-Bloch calculations on a single M_J ladder, I have tested Bloch solutions with four methods of simplification: (1) $M_J=1$ with $e\ ^3P_2$ state, (2) $M_J=1$ with $e\ ^3P_J$ effective Rabi rate, (3) $M_J=0$ with $e\ ^3P_2$ state, and (4) $M_J=0$ with ^3P_J effective Rabi rate. The effective Rabi rate is the geometric mean of the ^3P_J Rabi rates of DLM.[1] The results are very similar in the 3 to 10 GW/cm^2 region. From these I have selected the $M_J=1$ ladder with $\Omega_{eg}=3.74\ \mathrm{s}^{-1}$ per GW/cm^2 for use in the ensuing propagation calculations. In Fig. 3 I give the ionization probabilities for the $J=2$ to $J'=2$ transition as a function of laser peak intensity for a 0.3-ns FWHM Gaussian pulse. Three tunings of the laser are shown for a 0 K Doppler situation, and two tunings for an 800-K Doppler distribution. Also shown is the effect of replacing the $M_J=0,\pm 1$ ladders by just the $M_J=1$ ladder. The error is generally less than 15% in terms of ionization probability. When this "one-ladder" approximation is made, the ground-state number density is increased by a factor of 3 to compensate for the missing ladders.

The change in slope of the 0-K, zero-detuning curve in Fig. 3 occurs at the point in intensity where the density matrix begins to exhibit strong Rabi oscillations on the two-photon transition. The slope of all the curves at low intensity is three, reflecting the (2+1)-photon dynamics prior to the onset of saturation. The splitting of the -0.1- and 0.1-cm^{-1} detuning curves, as well as the crossing of the 0- and 0.1-cm^{-1} curves is a reflection of the intensity-dependent ac Stark shifts. The high-intensity portion of Fig. 3 will be in error if the intensity-dependent ac Stark shift (near 0.036 cm^{-1} per GW/cm^2 for all transitions) is sufficient to force $e\ ^3P_1$ into closer resonance with the applied field than the $e\ ^3P_2$ level. For an applied field with $+0.1$ cm^{-1} (laser) detuning from $^3P_2$, this intensity is 13 GW/cm^2; for zero detuning, the intensity break point is 7.5 GW/cm^2; for -0.1 detuning, the break is 2 GW/cm^2. The latter is particularly low because the two-photon laser is already tuned 0.2 cm^{-1} to the red on the transition, which is 0.2/0.54 of the separation of the $^3P_2$ and $^3P_1$ lines. The error due to the level shifting will not be important as the main thrust of this work is parametric growth in the situation that the laser is tuned to match the Stark-shifted $e\ ^3P_2$ line component.

At 800 K, the Doppler effect tends to smooth out the dependence of the ionization probability on pump laser frequency; this is shown by the two dashed curves in Fig. 3. In the operation region of interest (Sec. IV D), the Doppler effect gives less than a factor of 2 correction to the ionization probability.

D. Growth of parametric waves

The calculations of Sec. IV C show where one may expect efficient (2+1)-photon ionization of O. In Fig. 3 one sees that peak intensities from 3 to 10 GW/cm^2 with a laser detuning of 0.1 cm^{-1} are good. It is difficult to generate collimated beams at higher intensities, and moreover, the single resonant exicted state used in my computations is not a good approximation at very high intensities. The time-dependent ac Stark shift places the $g\ ^3P_2$-$e\ ^3P_2$ transition into exact resonance at the half-intensity points of a 5.56 GW/cm^2 peak-intensity pulse detuned by 0.1 cm^{-1} (laser) from the $J=2$, $J'=2$ fine structure line.

In Figs. 4–6, parts (a), I give the time behavior of the populations of the g, i, and e levels as well as the ion production for peak intensities of $10^{n/4}$ GW/cm^2 $n=2,3,4$ (i.e., 3.16,5.62,10 GW/cm^2). The ground level density is 2.5×10^9 cm^{-3}, which is 0.5×10^9 cm^{-3} in each M_J state, increased by a factor of 3 to compensate for the three, nearly equivalent, strongly coupled, $M_J=0,\pm 1$ ladders. These are numerical solutions of Eq. (7) responding to E_1 only. In Fig. 4–6, parts (b), I give the λ_+ growth "constant" for each of the intensities, evaluated from the density matrix as in Eq. (29). λ_+ is negative for all retarded times at 3.16 GW/cm^2, it increases to positive values at 5.62 GW/cm^2 with a positive tail due to the residual pop-

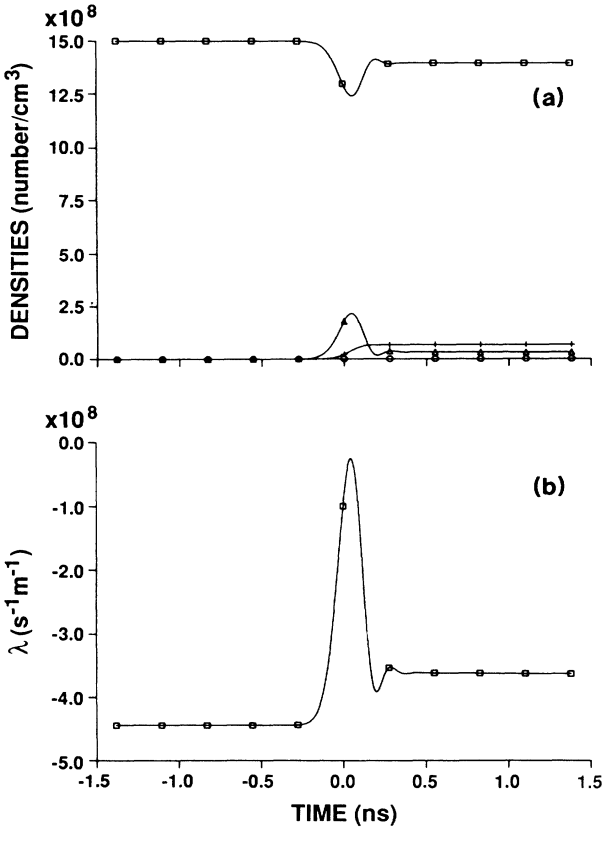

FIG. 4. In part (a) the number densities as a function of retarded time are given for the ground state (□), the intermediate state (○), the excited state (△), and the ions (+). In part (b), the FWM growth "constant" is given as evaluated from the density matrix as described in the text. These calculations were based on a 0.3-ns FWHM pulse with 3.16 GW/cm^2 peak intensity, tuned 0.2 cm^{-1} to the blue on the transition energy of the $J=2$ to $J=2$ line.

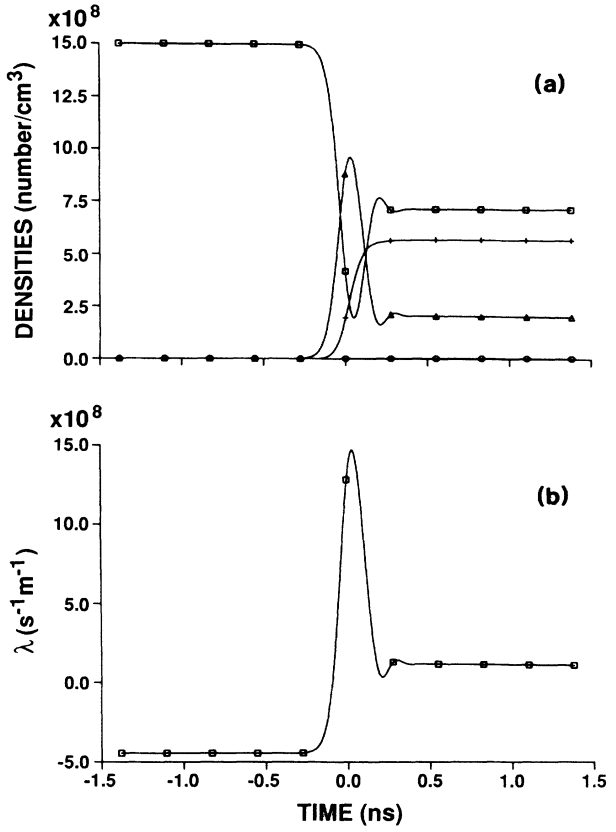

FIG. 5. Same as Fig. 4 except the peak pulse intensity is 5.62 GW/cm^2.

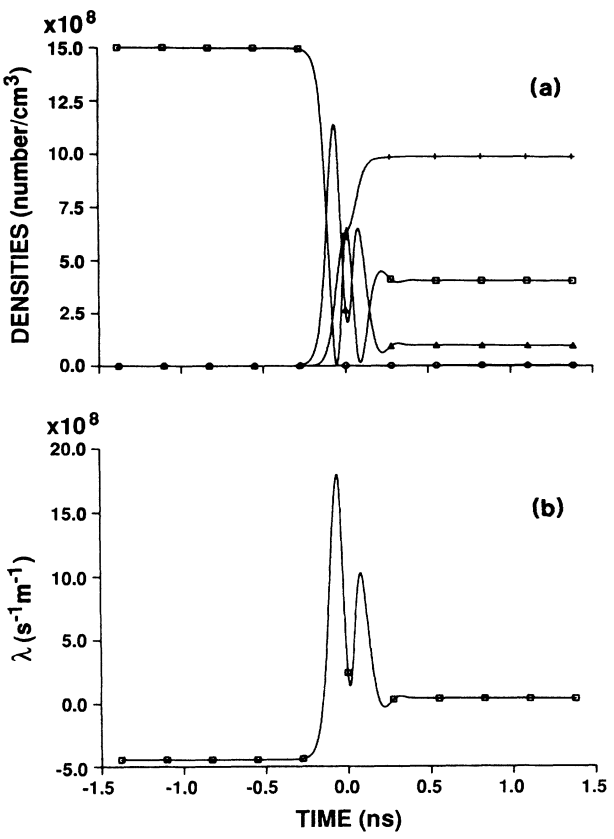

FIG. 6. Same as Fig. 4 except the peak pulse intensity is 10 GW/cm^2.

ulation left unionized in e, and it has a positive double peak at 10 GW/cm^2 in Fig. 6(b). The peak in Fig. 6(b) is not significantly greater than peak in Fig. 5(b). If the early growth theory of Sec. III is correct, this span of intensity from 3 to 10 GW/cm^2 should cover the transition region for the onset of parametric wave growth for the 0.3-ns, (2+1)-photon ionization of O.

The parametric fields are initialized at $z=0$ as smooth envelopes of carriers at the e to i and i to g frequencies. Exploratory calculations with random phase noise, random amplitude noise, and greatly disparate magnitudes did not affect the growth or nongrowth in any significant way. Because of the general nature of the carrier-amplitude factorization used here, the growing fields establish their phase matching subject only to the single major restriction that the propagation vectors are collinear. Figure 7 gives the intensity profiles used to initiate these particular propagation calculations. The peak I_2 and I_3 are 10^{-6} W/cm^2, and this I_1 peak is 10 GW/cm^2. The populations evolve at $z=0$ just as shown in Fig. 4–6 for the three peak intensities of I_1 chosen for study: 3.16, 5.62, and 10 GW/cm^2. At $z=100$ m, the intensities are given in Figs. 8–10 for the three cases. The extinction of the leading edge of the I_3 pulse is due to the interaction with the ground state prior to the atomic response to I_1. One notes the extensive pulse distortion of both I_2 and I_3. This pulse drag was noted in the ana-

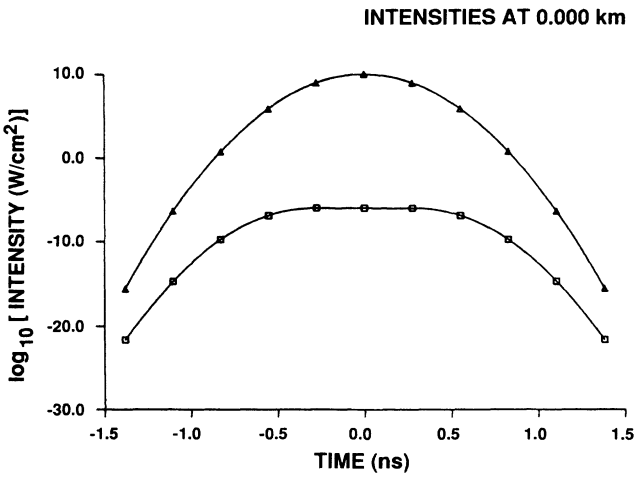

FIG. 7. Retarded time dependence of intensities of fields at $z=0$. The I_1 shown here (△) is a 0.3-ns FWHM Gaussian with a peak of 10 GW/cm^2. I_2 (□) and I_3 (○) coincide and are each a sum of Gaussians with peak value 1 μW/cm^2.

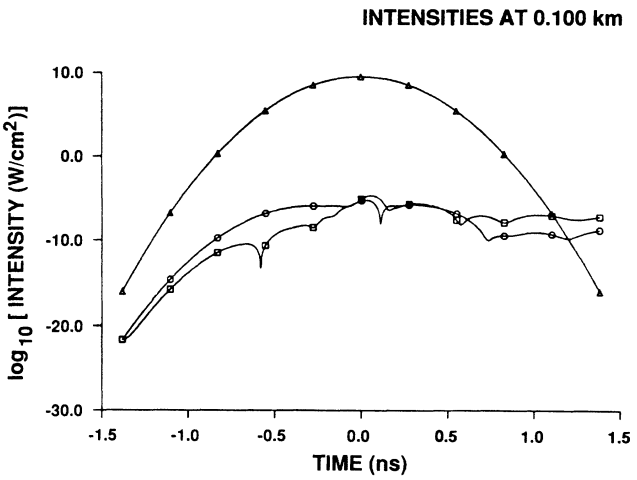

FIG. 8. Intensities at 100 m of propagation into a medium at 0 K. I_1, I_2, and I_3 are labeled △, ○, and □. This is peak I_1 of 3.16 GW/cm^2.

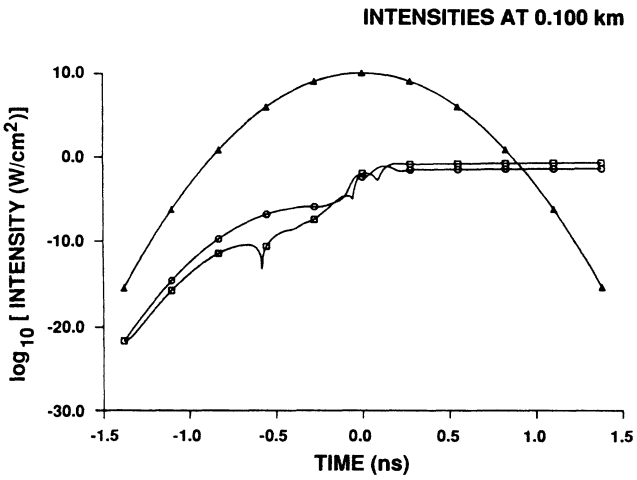

FIG. 10. Same as Fig. 8 except peak I_1 is 10 GW/cm^2.

lytic solutions to the early-growth regime in Sec. III B. It would be necessary to extend the retarded time range considerably in order to compute the tails of the growing waves. At $z=200$ m, Figs. 11–13 give the intensities. To be noted is the insignificant growth at 3.16 GW/cm^2, and the very abrupt onset of growth as a function of retarded time at the higher I_1 intensities.

The Doppler effect at 800 K shows the field growth as shown in Figs. 14 and 15 for $I_1=5.62$ GW/cm^2. The hole-burning effect is shown in Fig. 16 for this intensity and temperature. It is seen that the Doppler effect greatly inhibits the growth of the parametric waves.

A final point for computational exploration is the saturation of the parametric growth. The early growth is nearly exponential, but this quickly converts into linear growth where I_2 and I_3 become large enough to compete with I_1 in the driving of the atomic response. To avoid voluminosity, I present the results of the propagation calculations by showing the growth of the pulse fluences with distance; the intensity profiles generally retain the shapes of Fig. 12. The initial fluences, F_2 and F_3, of the injected pulses are $\sim 10^{-11}$ J/cm^2 (10^{-2} W/cm^2) in these calculations. The reported fluences are the time integral of the intensities of the computed fields over the retarded time interval shown in the figures. This measure of the wave growth contains some error as the pulses have not died off at the end of the retarded time interval. However, the effect of the parametric waves on the ionization process is totally contained in the displayed time interval. Recall that the ordinate scale is logarithmic on the intensity plots, so that the pulses are not so broad as appears. In Fig. 17 I show the nearly linear growth of I_2 and I_3 and the suppression of ion production for $I_1=4$ GW/cm^2. The transition region from exponential to

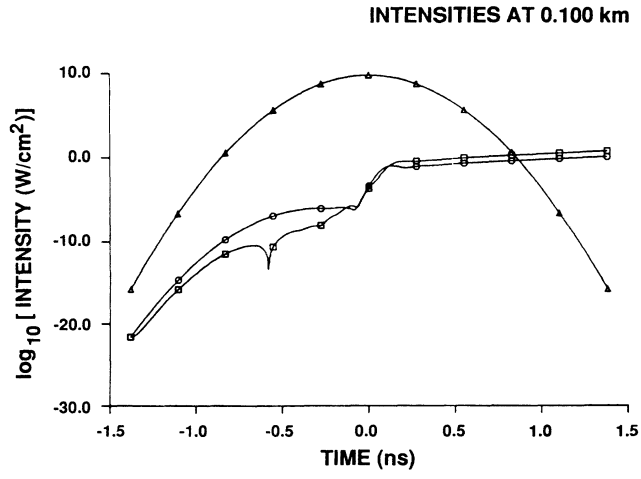

FIG. 9. Same as Fig. 8 except peak I_1 is 5.62 GW/cm^2.

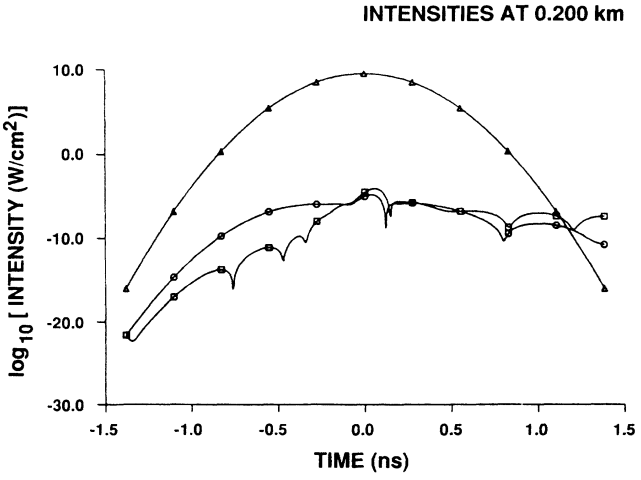

FIG. 11. Same as Fig. 8 except propagation distance is 200 m.

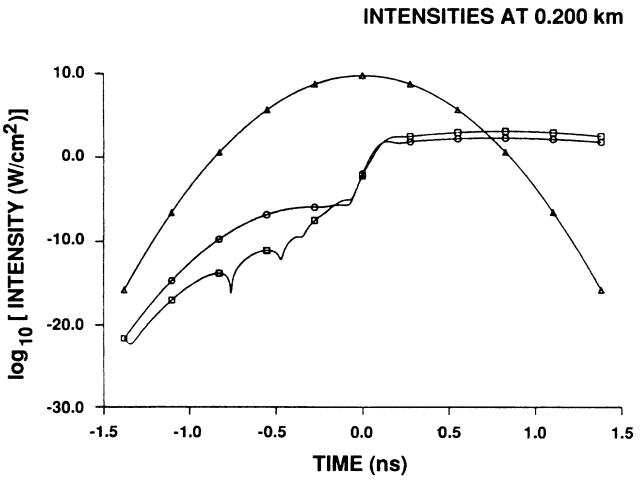

FIG. 12. Same as Fig. 9 except propagation distance is 200 m.

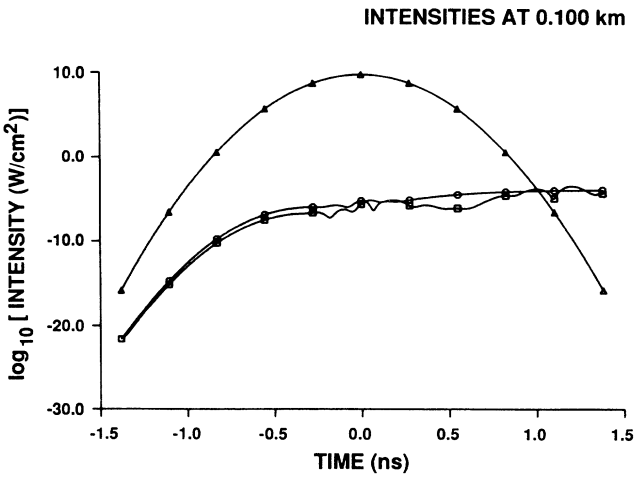

FIG. 14. Intensities at 100 m after propagation through Doppler-distributed medium at 800 K. This growth should be compared to Fig. 9 which did not include the Doppler effect. Peak I_1 is 5.62 GW/cm^2.

linear growth occurs where the growth of I_2 and I_3 reach roughly 10^2 to 10^3 W/cm^2 and F_2 and F_3 are about 10^{-7} to 10^{-6} J/cm^2.

The limiting form of saturated wave growth and density matrix evolution is difficult to analyze analytically. Generally, I expect the traveling-wave solutions to settle into stable waveforms of slow z' dependence. With this assumption, the dipole densities driving E_2 and E_3 should nearly vanish [Eq. (16)], and this implies from Eq. (18) that

$$|E_3|^2/|E_2|^2 \approx |D_{ei}|^2 \rho_{ee}/|D_{ig}|^2 \rho_{gg} \ . \tag{55}$$

The ratio of I_3 to I_2 in the early growth region is given by Eq. (40). Combining Eqs. (40) and (55) leads to the statement that growth suppression is contingent upon photon-number balance in fields 2 and 3:

$$|E_3|^2/\hbar\omega_3 \approx |E_2|^2/\hbar\omega_2 \ . \tag{56}$$

This in turn may be combined with Eq. (55) to show that λ_+ of Eq. (29) should be suppressed to zero. I interpret this to mean that the fields 2 and 3 evolve to affect the density matrix such that their growth constant (λ_+) is suppressed, resulting in the observed linear behavior in the larger propagation distances in Fig. 17. Examination of λ_+ at these distances (not shown) indeed shows that it is driven into rapid oscillation about a zero mean. Thus the above arguments are supported by the calculations. The ionization fraction of atomic oxygen is seen to stabi-

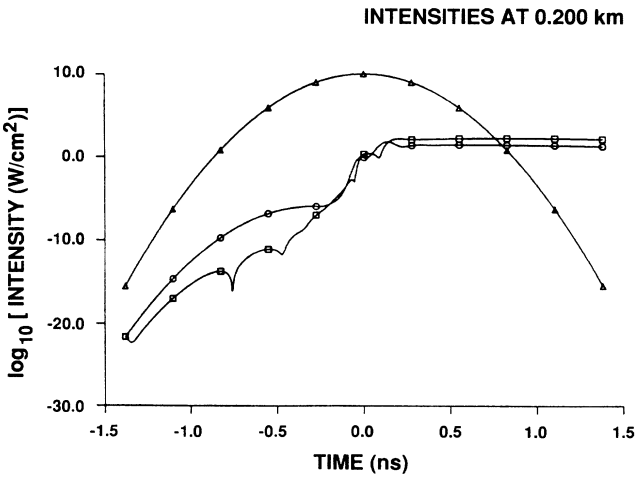

FIG. 13. Same as Fig. 10 except propagation distance is 200 m.

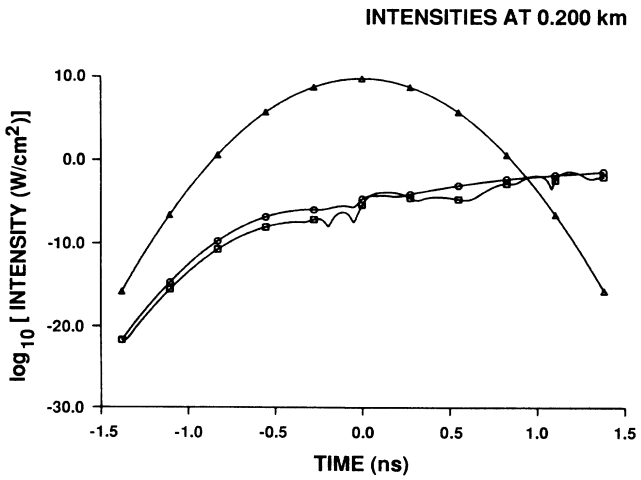

FIG. 15. Same as Fig. 14 except propagation distance is 200 m. This should be compared to Doppler-free (i.e., 0 K) results given in Fig. 12 for peak I_1 of 5.62 GW/cm^2.

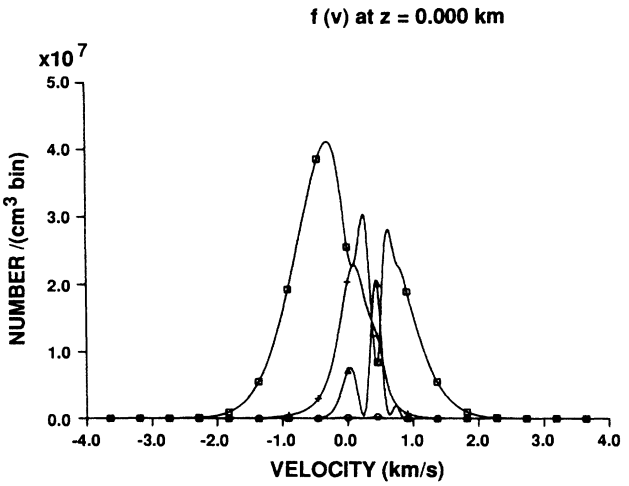

FIG. 16. Velocity distributions of ground state (□), intermediate state (○), excited state (△), and ions (+) at the beginning of channel for peak I_1 of 5.62 GW/cm^2 after passage of laser pulse.

lize around 0.05 in Fig. 17; other calculations demonstrate analogous suppression of ionization, with the density matrix settling into a highly overdriven mode of oscillation at large propagation distances.

The spectral density of the growing fields has been found by Fourier analysis of the computed pulse envelopes. The spectral densities are generally localized about the transition frequencies. In the early growth region for the case of a pump pulse peak intensity of 5.62 GW/cm^2 detuned 0.1/cm^{-1}, the e to i (ω_2) transition shows a growth shifted to higher frequency, probably due entirely to the ac Stark effect of the pump, which predominantly affects the e level. The later stages of growth show a breakup of the spectrum of the I_2 and I_3 fields on the order of a few GHz, with the amount of breakup increasing with distance (thus strength of the E_2 and E_3 fields).

V. DISCUSSION

The growth of parametric fields (FWM and ASE) in two-photon excitation is a complex phenomenon. This work is directed toward the short, on-resonant, intense pulse limit of a (2+1)-photon process for producing channels of ionized atomic oxygen. The earlier work of BMGR (Ref. 2) was directed toward a long, weaker pulse regime in alkali vapor in which the results were quite distinct from the present. Whereas I find partial suppression of excitation and ionization due to the growing fields for $\lambda_+ > 0$, BMGR predict complete suppression of the (2+1)-photon process.

The early growth theory used here in Sec. III can be extended to the perturbational limit used by BMGR, with the major difference being my retention of the single-photon coupling terms (in the Bloch equation) to the states. With this coupling retained in the analysis, the conditions for wave growth with distance are different, displaying a threshold similar to Eq. (29).[12] The origin of this threshold is the competition between the FWM growth and linear absorption of ω_3 by the ground state.

As to the experimental verification of a threshold for the FWM onset and the amount of suppression of excitation, one must verify that the theoretical analysis presented here applies to the physical problem. I have assumed short, transform-limited pulses, collisionless atoms, and a moderately important Doppler effect.

In the situation which I am addressing in the high atmosphere, it appears that 0.3-ns pulses of less than 3 GW/cm^2, detuned to the ac-Stark-shifted position of the $g\ ^3P_2$-$e\ ^3P_2$ fine-structure line, will produce channels of ionization without significant degradation due to FWM growth.

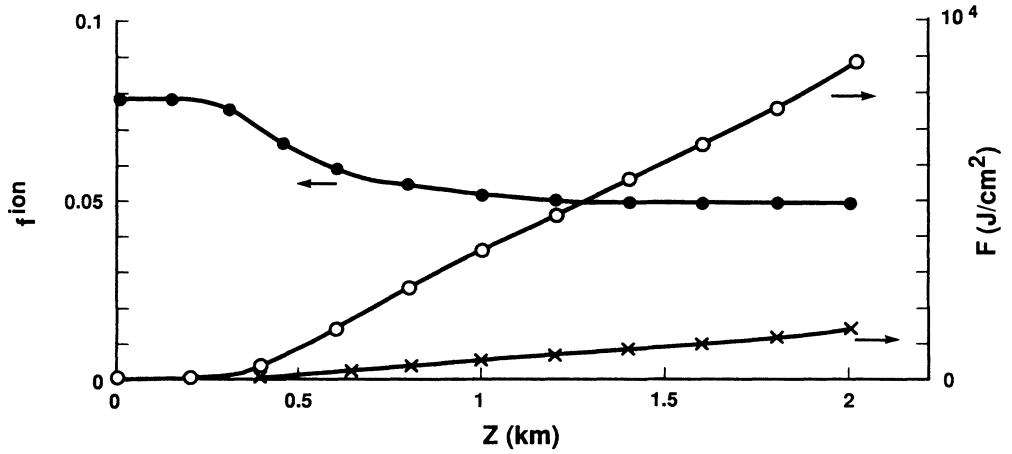

FIG. 17. Growth of pulse fluences [I_2 (-×-) and I_3 (-○-)] and decrease in ionization fraction for 0 K case with a 0.3-ns Gaussian I_1 with peak intensity of 4 GW/cm^2. The linear growth region is characterized by nearly equal photon densities in the I_2 and I_3 fields. The very slight change in slope at the 2-km point may be numerical error.

ACKNOWLEDGMENTS

The author is appreciative of many helpful duscussions with Arlee Smith concerning four-wave mixing. This work was performed at Sandia National Laboratories and supported by the U.S. Department of Energy under Contract No. DE-AC04-76DP00789.

[1]S. N. Dixit, D. A. Levin, and B. V. McKoy, Phys. Rev. A **37**, 4220 (1988).

[2]R. W. Boyd, M. S. Malcuit, D. J. Gauthier, and K. Rzazewski, Phys. Rev. A **35**, 1648 (1987).

[3]A. Icsevgi and W. E. Lamb, Jr., Phys. Rev. **185**, 517 (1969).

[4](a) B. A. Capron and M. Sargent III, Phys. Rev. A **34**, 3034 (1986); (b) A. Guzman de Garcia, P. Meystre, and R. R. E. Salomaa, Phys. Rev. A **32**, 1531 (1985); (c) S. N. Dixit and P. Lambropoulos, Phys. Rev. A **27**, 861 (1983); (d) P. W. Milonni and J. H. Eberly, J. Chem. Phys. **68**, 1602 (1978); (e) D. Grischkowsky, M. M. Loy, and P. F. Liao, Phys. Rev. A **12**, 251 (1975).

[5]T. J. McIlrath, R. Hudson, A. Aikin, and T. D. Wilkerson, Appl. Opt. **18**, 316 (1979).

[6]D. J. Bamford, L. E. Jusinski, and W. K. Bischel, Phys. Rev. A **34**, 185 (1986).

[7]I. I. Sobel'man, *Introduction to the Theory of Atomic Spectra* (Pergamon, Oxford, 1972).

[8](a) C. E. Moore, *Atomic Energy Levels,* Natl. Bur. Stand. Circ. No. 467 (U.S. GPO, Washington, D.C., 1949); (b) W. L. Wiese, M. W. Smith, and B. M. Glennon, *Hydrogen Through Neon,* Vol. 1 of *Atomic Transition Probabilities,* Natl. Bur. Stand. Ref. Data Ser., Natl. Bur. Stand. (U.S.) Circ. No. 4 (U.S. GPO, Washington, D.C., 1966).

[9]D. B. Jenkins, J. Quant. Spectros. Radiat. Transfer **34**, 55 (1985).

[10]*Survey of Numerical Analysis,* edited by J. Todd (McGraw-Hill, New York, 1962).

[11]M. E. Riley, T. D. Padrick, and R. E. Palmer, IEEE J. Quant. Electron., **QE-15**, 178 (1979).

[12]R. W. Boyd, M. G. Raymer, P. Narum, and D. J. Harter, Phys. Rev. A **24**, 411 (1981).